

A climatological study of the influence of synoptic-scale flows on sea breeze evolution in the Bay of Alicante (Spain)

C. Azorin-Molina · D. Chen

Received: 2 July 2007 / Accepted: 13 March 2008
© Springer-Verlag 2008

Abstract The focus of this study is on sea breeze (SB) characteristics during May and August in the Bay of Alicante (south-eastern coast of the Iberian Peninsula, IP, Spain) for the period 2000–2005 in relation to dominating synoptic-scale winds. A dataset containing 292 SB events was objectively constructed to study the impact of the daily synoptic winds at 850 hPa on the main characteristics of SBs. The winds were used to designate three major synoptic-scale regimes: offshore, onshore, and coast-parallel flows. The SB features examined include mean lag of the SB passage, wind speed and direction at the time of onset, mean lag of SB cessation, mean duration of SB, mean maximum velocity, and inland propagation of SB. Some of the characteristics had not been previously considered in the literature. It is found that in comparison with onshore synoptic flows, offshore favors the delayed arrival and termination of SBs, resulting in a longer mean duration. Further, they produce the most intense passages, cause a more frequent southeasterly component, and result in a higher SB gust speed and shorter mean inland penetration.

Results from coast-parallel flows are also presented. The strength of the large-scale flows plays a major role upon SB parameters, which essentially support other numerical modeling results.

1 Introduction

SBs are controlled by local and regional environmental factors influencing their development, evolution, and characteristics. Carnesoltas (2002) classified these factors into two main categories: (a) geographical-physical factors such as latitude (Yan and Anthes 1986), season, shape-curvature (convex or concave) and coastline orientation (McPherson 1970), distance between opposite coasts (Haurwitz 1947), land–sea boundary, depth of water, topography (Kusuda and Alpert 1983; Darby et al. 2002; Miao et al. 2003), land use (Baker et al. 2001; Miao et al. 2003), surface roughness, thermo-conductive and transmitter properties of terrain, and (b) meteorological, hydrological and oceanic factors such as direction and strength of the synoptic-scale flow, stability of the air mass (low level inversions), cloud cover, soil moisture, swell types and stream of water, and sea surface temperature (SST), (Bowers 2004). The first category is static or changes very slowly, whereas the second one alters within a few days and the meteorological parameters vary from day to day or even from hour to hour.

SBs are primarily driven by local sea and land air temperature difference (ΔT), which is directly related to pressure difference. Previous SB studies have shown that SB intensity is directly proportional to local solar radiation. Mesoscale environmental factors other than ΔT have nonetheless been found to play a major role in controlling SB characteristics (Borne 1998). The overlying synoptic-

C. Azorin-Molina (✉)
The CEAM Foundation (Fundación Centro de Estudios Ambientales del Mediterráneo), Parque Tecnológico,
Charles R. Darwin 14,
46980 Paterna, Valencia, Spain
e-mail: cazorin@ceam.es

C. Azorin-Molina
Group of Climatology, University of Barcelona,
Montalegre 6,
08001 Barcelona, Catalonia, Spain

D. Chen
Regional Climate Group, Department of Earth Sciences,
Göteborg University,
405 30 Göteborg, Sweden

scale flow is by far the most influential factor in the characteristics and occurrence of an SB.

The interaction between large-scale synoptic winds and SBs has been well documented (e.g., Zhong and Takle 1993) by many numerical-theoretical (Estoque 1962; Pielke 1974; Simpson et al. 1977; Bechtold et al. 1991; Arritt 1993; among others) and observational (Wexler 1946; Frizzola and Fisher 1963; Abbs 1986; Atkins and Wakimoto 1997; Gilliam et al. 2004; among others) investigations. The impact of large-scale flows is greater than the thermal gradient caused by heating during the daytime (SB phase; Salvador 1999).

The wind direction (WD) of large-scale flows plays an important role in the evolution of SBs. Previous studies have shown that a perpendicular offshore large-scale wind strengthens SB perturbation by compressing the horizontal land–sea temperature gradient. Onshore geostrophic winds disturb this thermal gradient and consequently weaken SBs. Coast-parallel or antiperpendicular large-scale flows are hybrids of the offshore and onshore winds and therefore have an intermediate effect on SB evolution (Gilliam et al. 2004), despite the fact that few episodes have been analysed (Atkins and Wakimoto 1997).

The wind speed (WS) of ambient gradient flows also plays a significant role as it controls the momentum of the disturbances on the horizontal plane. A strong large-scale flow produces a weaker concentration of these disturbances and smoothes the peaks of the perturbation (Walsh 1974). SBs alter significantly when the WS of ambient gradient flows changes (Bechtold et al. 1991). Maximum SB gust speed occurs when the propagation speed of SB fronts is cancelled by large-scale offshore WS (Bechtold et al. 1991; Zhong and Takle 1993).

Despite the existing studies, the impact remains to be fully understood (Atkins and Wakimoto 1997), which requires more detailed research into SB characteristics as a function of prevailing low-level synoptic flows. Previous numerical-theoretical and observational investigations have only studied a few events over flat terrain for SB simulations. Here we use a large number of SB episodes to develop a climatological study of the effects of large-scale flows influencing the characteristics of SBs over a complex land-sea interface.

Weak geostrophic wind (Wg), anticyclonic circulation, intense solar radiation and clear skies are the typical meteorological conditions ensuring the high persistence of SBs in the Western Mediterranean Sea (Ramis and Alonso 1988; Ramis and Romero 1995). An SB occurs on two out of every three days in the Bay of Alicante (Azorin-Molina and Martin-Vide 2007). The study of SB characteristics in relation to synoptic-scale flows is important due to their influence on air pollution transport and diffusion; initiation, location, and intensity of convection (SB frontogenesis);

forest fire forecasting; agriculture (Bonnardot et al. 2005); aviation safety; gliding and sailing; among other things (Simpson 1994).

A large number of statistics including onset-lag, onset-speed, onset-direction, cessation-lag, duration, maximum gust speed, and inland penetration of SBs were studied herein. The purpose is to gain a better understanding of SB interaction with synoptic-scale winds in the region. Due to the climatological nature of the study, the results can be readily used to test some hypotheses presented by numerical studies in the literature.

2 Data and methods

2.1 Study area and data set

Figure 1 shows the topography features of the province of Alicante: a portion of the southeastern Mediterranean coast and adjacent inland areas of the Iberian Peninsula (IP), located in the Western Mediterranean Sea between 37°51'N and 40°48'N and 1°32'W and 0°31'E. The terrain is quite complex, with coastal plains, valleys and the Prebetic mountain ranges (1,000–1,600 m). The general shape-curvature of the coastline is concave, even though local convex (capes) and concave (bays) land–water boundaries are present within the province. The study focuses on the Bay of Alicante.

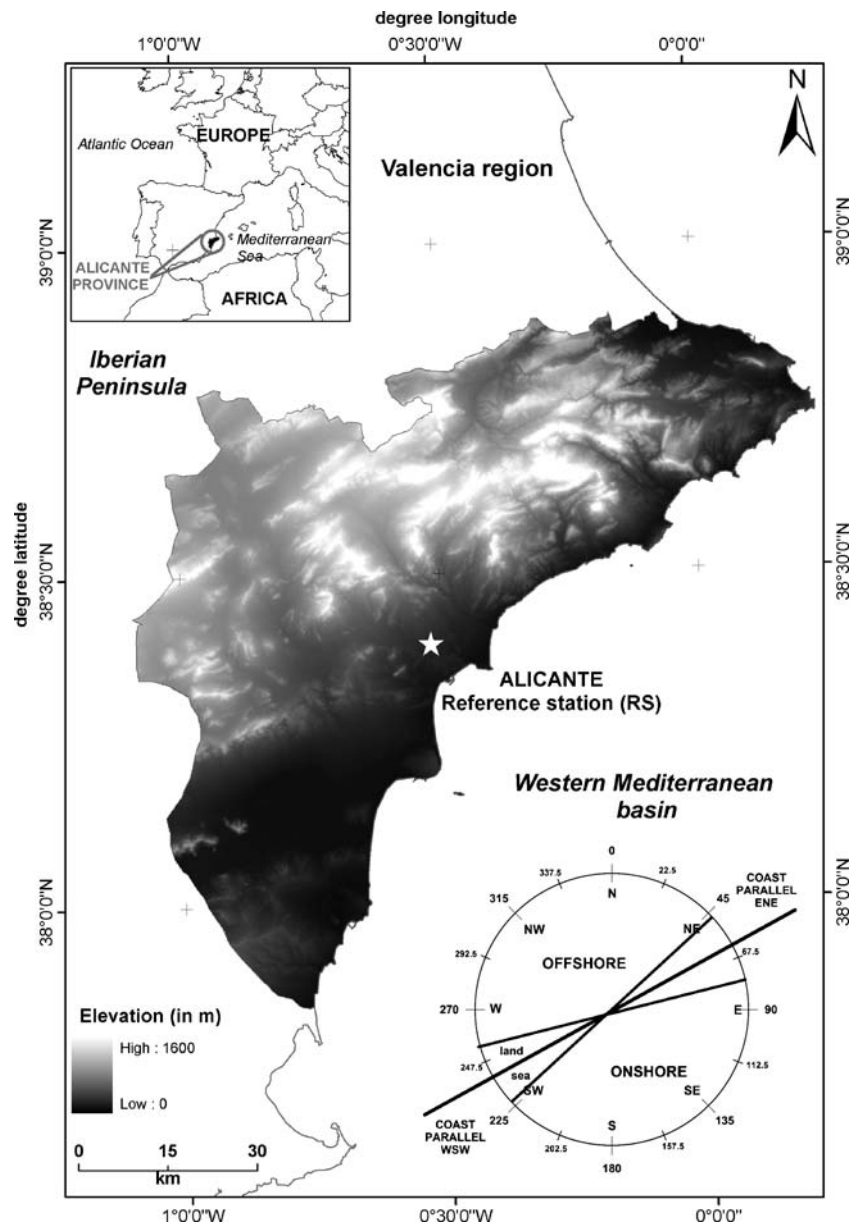
Alicante's meteorological station (Laboratory of Climatology, University of Alicante; <http://www.labclima.ua.es/>) was chosen as the reference synoptic station (RS). The Alicante station (38°23'N and 0°31'W; 102 m a.s.l) is situated 5.1 km from the coast with a concave coastline (Bay of Alicante), where the coastal mountain ranges are located between 10 and 15 km inland. The surface meteorological observations used here consist of 30-min WS (in m s^{-1} units) and WD (in $^{\circ}$ units and stored in 1° steps) data. The shoreline is oriented 62–242° and the sea and land-breeze central axes are therefore from 152° and 332°, respectively.

This study focuses on the May–August period and attempts to discriminate the influence of the seasonal physical-factor on SB characteristics. The difference in radiation forcing is around 15% in this period, largest around June 21st and smallest at August 31st. The amount of energy reaching a square metre is around 95.0% of the maximum possible on June 21st.

2.2 SB data set and statistics

An automatic and objective method to identify SB can be used to screen the observation data for computing SB statistics (Borne et al. 1998). The automated method used

Fig. 1 Topographic map of the province of Alicante showing the surface meteorological station (RS) in the Bay of Alicante. WD of the four regimes are shown in the lower right corner



here for identifying past SB events is based on two filter groups: (a) distinctive features in WD and WS, and (b) physical processes of SBs. The first filter group uses the characteristic abrupt shift in WS and WD associated with the initiation and cessation-time, and the maximum WS (WS_{max}) of SBs. The second filter group employs a filter based on the semi-diurnal pressure wave or diurnal air pressure amplitude (Prtenjak and Grisogono 2007) in combination with a positive difference in temperature between the daily maximum at the RS and the SST ($\Delta T > 0^\circ\text{C}$, Laird et al. 2001). A detailed account of the objective selection technique is described in Azorin-Molina (2007). A subset of 292 SB events was found in the RS after applying the automatic scheme from May to August for the 6-year period (2000–2005). The following charac-

teristics of the SB have been computed for each episode in relation to large-scale synoptic winds:

- (I) *Onset*: The onset is defined by the SB passage between 01 and 7:30 h after sunrise. The onset occurs when the 30-min mean WS (WS_x) is equal or higher than 1.5 m s^{-1} and the 30-min mean WD (WD_x) is from 45.0° to 180.0° at the same time. Previous WS_x and WD_x must be less than 1.5 m s^{-1} or from 181.0° to 44.0° (land breeze), respectively. The onset-lag (O_{lag}), onset-speed (O_{ws}) and onset-direction (O_{wd}) have been studied in this work. The hypotheses to be tested are: (a) The O_{lag} is greater and (b) the O_{ws} is relatively higher due to offshore large-scale synoptic winds than onshore ones. The O_{wd} behavior is studied for the first

time under synoptic-scale flows, and had not previously been regarded in the literature.

- (II) *Cessation*: The cessation is defined by the SB front retreat between 01 h before and 05 h after sunset. The cessation-lag (C_{lag}) happens when WS_{max} is less than 1.5 m s^{-1} or WD_x is from 226.0° to 44.0° (land breeze). No study of this parameter in relation to background winds has been reported before.
- (III) *Temporal dimension or duration (D_t)*: Period of time between the onset and cessation time of SBs. This SB feature had not been studied before, either.
- (IV) *Maximum velocity*: WS_{max} is the maximum WS reached in the SB period. The hypothesis to be tested is: The SB exhibits the strongest WS_{max} on days controlled by offshore gradient winds.
- (V) *Inland penetration (SB_{ext})*: The horizontal extent of SBs was calculated as follows (Salvador and Millan 2003):

$$SB_{ext} = \sum \sqrt{u^2 + v^2} * \Delta t \quad (1)$$

where u and v are the west–east and north–south components (Stull 1995) of SBs and Δt is equal to the interval of time in which the wind data were stored, i.e., 30 min. This equation measures the distance that a particle travels if the vector wind is constant along its displacement. This provides a first-order estimation of the inland propagation of SBs using a single observation point and without considering topography, which can have strong local effects (Simpson 1994). The hypothesis to be tested is: The horizontal extent of SBs is reduced under offshore large-scale winds.

2.3 Synoptic-scale flow regimes

The daily 850 hPa u -wind and v -wind data from the National Centers for Environmental Prediction (NCEP) and the National Center for Atmospheric Research (NCAR) reanalysis project (<http://www.cdc.noaa.gov/cdc/reanalysis/>

[reanalysis.shtml](#); Kalnay et al. 1996) were used to designate the synoptic-scale flow regimes. The grid-point at 357.5°W – 37.5°N was chosen as the closest site that best represents the impact of low-level synoptic-flows on SB characteristics in the Bay of Alicante. Additionally, the 850-hPa wind was assumed to be representative of the low-level synoptic forcing on local winds because the layer 0–1,500 m is the one where SBs develop (Banta et al. 1993; Helmis et al. 1995).

Even though the Bay of Alicante is concave, the reanalysis wind data were then classified into four main flow typologies taken an orientation 62.0° to 242.0° : (a) offshore winds (257.1° – 46.9°), which are large-scale flows from land to sea, (b) onshore flows (77.1° – 226.9°) which correspond to synoptic-scale flows from sea to land, (c) coast-parallel WSW winds (227.0° – 257.0°), which are low-level flows with land on the left, and (d) coast-parallel ENE flows (47.0° – 77.0°), which are low-level winds with land on the right. The surface friction produces a weak onshore and offshore component for the WSW and ENE flows, respectively. In theory, SBs that develop under the ENE winds have characteristics of the offshore flows whereas the WSW flows correspond to the onshore winds (Zhong and Takle 1993; Nuss 2005; Weaver 2006). An inset diagram of the synoptic-scale flow regimes is displayed in Fig. 1. Each of the four main regimes was sub-classified into light to moderate (Lm, $\leq 5.14 \text{ m s}^{-1}$) and strong (Str, $> 5.14 \text{ m s}^{-1}$) categories according to Gould and Fuelberg (1996) and Connell et al. (2001). Onshore synoptic-scale flows are the most frequent regime covering 55.5% of SB episodes (49.0% of the days during May and August for the 6-year period 2000–2005). Offshore large-scale winds are less frequent, with 25.7% in SB episodes (32.9% from May to August 2000–2005). The coast-parallel WSW regime contains 13.7% (6 year: 13.7%), whereas the coast-parallel ENE category 5.1% (6-year: 4.3%) of SB days (Table 1).

The strongest synoptic-scale flow is 9.6 m s^{-1} for SB episodes, while the class intervals of 3.1 – 4 m s^{-1} (18.5%) and 4.1 – 5 m s^{-1} (16.8%) are frequent. These intervals also

Table 1 Distribution of absolute (n_i), relative ($n_i, \%$) and collated relative frequencies ($\Sigma n_i, \%$, in bold type) of SB episodes (Sb) and days for the 6-year study period (2000–2005; from May to August) by

Flow regime		Offshore		Onshore		Coast-parallel ENE		Coast-parallel WSW	
		Lm	Str	Lm	Str	Lm	Str	Lm	Str
Sb	n_i	61	14	109	53	13	2	23	17
	$n_i, \%$	20.9	4.8	37.3	18.2	4.4	0.7	7.9	5.8
	$\Sigma n_i, \%$	25.7		55.5		5.1		13.7	
6 years	n_i	152	91	238	124	25	7	50	51
	$n_i, \%$	20.6	12.3	32.2	16.8	3.4	0.9	6.8	6.9
	$\Sigma n_i, \%$	32.9		49.0		4.3		13.7	

means of the light and moderate (Lm, $\leq 5.14 \text{ m s}^{-1}$) and strong (Str, $> 5.14 \text{ m s}^{-1}$) flow regimes

represent a turning point for the occurrence of SBs: the dominant part of the breeze occurrence depends upon WS being below these intervals. Kwiatkowski (1999) observed that an offshore-directed wind of 10 m s^{-1} was sufficient to allow SB development in New Jersey. Savijärvi and Alestalo (1988) and Arritt (1993) set the threshold value of the W_g from which the SB does not develop at 8 m s^{-1} and 11 m s^{-1} , respectively. These studies computed the W_g at the surface level.

The 292 SB days with similar low-level regimes were then grouped together and the results concerning the impact of synoptic flows on SB characteristics are described in Sect. 3.

3 Results

3.1 The onset features of the SB

3.1.1 Mean lag of the SB passage (O_{lag})

The times of sunrise (in UTC) from May to August in the RS were used in order to compute the O_{lag} . The sunrise varies from as early as 04 h 37' UTC during the summer solstice to 05 h 30' UTC at the end of August. The O_{lag} parameter explains the SB initiation in relation to the synoptic-scale regimes better than the mean time of onset (O_t), since it is directly influenced by solar heating. The mean time of onsets (08 h 53' UTC) which is the average of 08 h 54' UTC (offshore), 08 h 50' UTC (onshore), 09 h 06' UTC (coast-parallel ENE) and 09 h 00' UTC (coast-parallel WSW), is not used as it is mainly influenced by the season factor. The mean O_{lag} is 04 h 00', which is comparable to

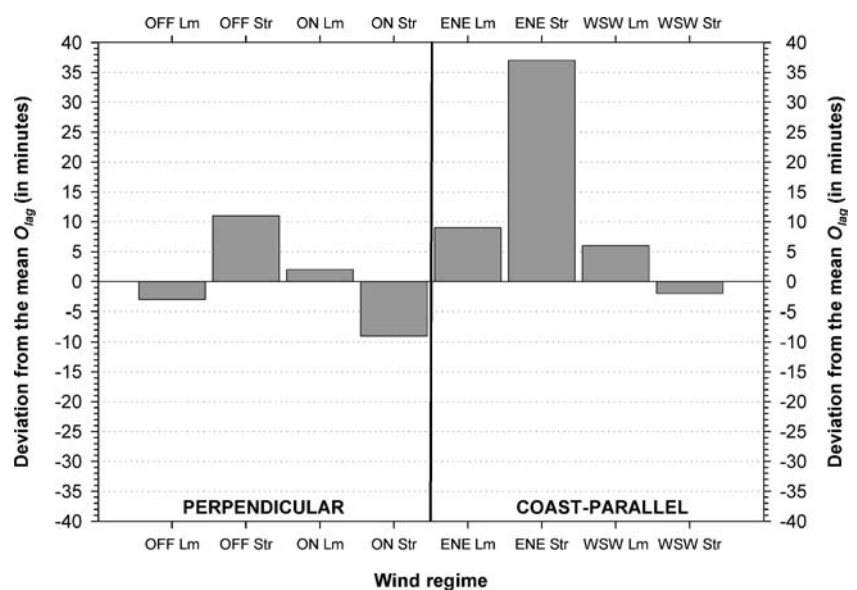
other published works (Atkinson 1981; Furberg et al. 2002). The maximum lag is 06 h 25' and the minimum is 01 h 22'. The lag is due to the time taken for vertical and horizontal adjustment of the atmospheric boundary layer across the shoreline (Furberg et al. 2002). The differences between the lags and the O_{lag} are 00' for offshore wind (04 h 00'), -02' for onshore wind (03 h 58'), 13' for coast-parallel ENE (04 h 13'), and 03' for coast-parallel WSW (04 h 03'), respectively.

It is also of interest to break down these four major synoptic-scale flows into light to moderate ($\leq 5.14 \text{ m s}^{-1}$) and strong ($> 5.14 \text{ m s}^{-1}$) categories. The main result is that the strength of synoptic-scale flows reinforced the results presented for the four regimes. Figure 2 displays the deviations of the lags for the eight regimes from the mean O_{lag} (in minutes). Strong offshore flows delayed the initiation of SBs 11' (04 h 11') than weak offshore ambient winds (-03'; 03 h 57'), (Asimakopoulos et al. 1999). An earlier SB onset was developed during strong onshore flows (-09'; 03 h 51') than light to moderate winds (02'; 04 h 02'). Interesting results have been provided through analysis of coast-parallel flows. The greatest delay in the arrival of SBs occurred under strong coast-parallel ENE winds (37'; 04 h 37'), which is 09' (04 h 09') for the ENE light to moderate flows. Likewise, with weak WSW low-level winds the SB passage came later (06'; 04 h 06') than strong flows from the same compass point which developed an early SB onset (-02'; 03 h 58 h).

3.1.2 Wind speed of the SB passage (O_{ws})

The WS_x at the time of an SB initiation (O_{ws}) was computed for each episode and their intensities were classified into six

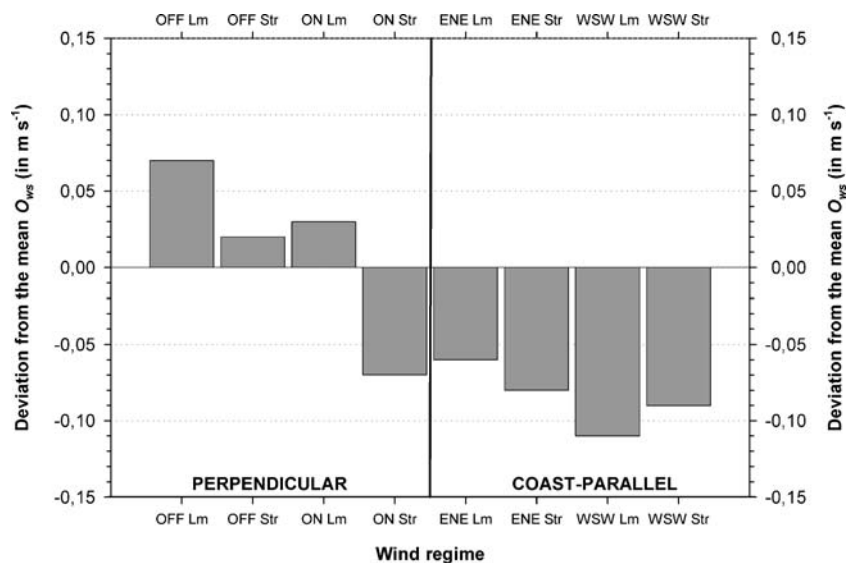
Fig. 2 Deviation of the mean lags of SB initiation for the eight synoptic-scale flows from the mean O_{lag} . The abscissa axis (X) represents the perpendicular (offshore, OFF, and onshore, ON) and coast-parallel (ENE and WSW) wind regimes by means of the light and moderate (Lm, $\leq 5.14 \text{ m s}^{-1}$) and strong (Str, $> 5.14 \text{ m s}^{-1}$) flow intensities



groups. The relative frequencies of each interval as represented by the mean O_{ws} for each group are as follows: 55.5% for 1.8 m s^{-1} , 29.8% for 2.2 m s^{-1} , 10.6% for 2.7 m s^{-1} , 2.1% for 3.1 m s^{-1} , 1.4% for 3.6 m s^{-1} and 0.6% for 4.0 m s^{-1} . The mean O_{ws} is 2.08 m s^{-1} for all SB events. Offshore large-scale flows tend to strengthen the mean O_{ws} (2.14 m s^{-1} , i.e., 0.06 above the mean), onshore synoptic-scale flows do not show any difference (2.08 m s^{-1}), whereas coast-parallel ambient winds seem to weaken local wind circulation (ENE 2.02 m s^{-1} and WSW 1.98 m s^{-1} , i.e., 0.06 m s^{-1} and 0.10 m s^{-1} below the mean, respectively). Despite the mean differences are very small, these results tally reasonably with the hypothesis put forward. The offshore geostrophic flows compress the horizontal land–sea temperature gradient (Arritt 1993).

Figure 3 displays the deviations of the mean WS at the time of onset for the eight regimes from their average. The mean O_{ws} was lower when the geostrophic wind was increased. This figure presents evidence that light to moderate offshore and onshore winds strengthened the mean O_{ws} to 2.15 m s^{-1} and 2.11 m s^{-1} , i.e., 0.07 m s^{-1} and 0.03 m s^{-1} above the mean O_{ws} , respectively. In contrast, strong offshore and particularly onshore flows weakened the SB mean WS at the time of onset to 2.10 m s^{-1} (0.02 m s^{-1} from the mean) and 2.01 m s^{-1} (-0.07 m s^{-1} from the mean), respectively. The coast-parallel flows from the ENE also weakened the mean O_{ws} to 2.02 m s^{-1} (-0.06 m s^{-1} from the mean) and 2.00 m s^{-1} (-0.08 m s^{-1} from the mean) for both light to moderate and strong winds, respectively. These differences are also slightly negative for the coast-parallel winds from the WSW with 1.97 m s^{-1} (-0.11 m s^{-1} from the mean) for light to moderate and 1.99 m s^{-1} (-0.09 m s^{-1} from the mean) for strong flows aloft.

Fig. 3 Deviation of the mean wind speed of SBs at the time of onset for the eight synoptic-scale flows from the mean O_{ws} . The wind regimes shown along the X axis are the same as in Fig. 2



3.1.3 Wind direction of the SB passage (O_{wd})

Figure 4 shows a polar bar chart of the relative frequency distribution (n_i , %) of the WD at the time of SB initiation for (a) the onshore and (b) offshore regimes. The general feature is that supporting synoptic-scale flows produced an O_{wd} from the 1st quadrant (from 45.0° to 90.0°). The maximum relative frequency distribution (28.4%) corresponds to the SB passages from the ENE (67.5°) whereas the O_{wd} from the E (90°) stands at 25.9%. For offshore large-scale winds the O_{wd} shifted from the 1st quadrant to the 2nd one (from 112.5° to 157.5°), with a maximum relative frequency distribution of 21.3% for the ESE (112.5°) direction. The O_{wd} from the SE (135°) also have a high relative frequency at 20.0%. Coast-parallel flows from the ENE and the WSW produce maximum relative frequency distribution of 33.3% and 22.5% for the ESE (112.5°) direction, respectively. The results for the eight regimes confirm this behavior (Table 2). For example, strong offshore flows tended to produce an O_{wd} from the SE (135°).

3.2 Mean lag of the SB cessation (C_{lag})

The time of the sunsets (UTC) was also used for computing the mean lag of the cessation of the SB (C_{lag}). The mean delay of SB retreat is 01 h 47', i.e., the SB is still blowing for almost 02 h after sunset (mean time of cessation or C_t is 21 h 02' UTC). The maximum C_{lag} is 04 h 53' (until 23 h 30' UTC) and less than 5% of SBs (12 episodes) ceased within 01 h of sunset (18 h 30' UTC). The statistics show quite a clear impact of synoptic-scale flows on the C_{lag} . Offshore large-scale winds delayed the cessation of this local wind by 07' (C_{lag} is 01 h 54', i.e., until 21 h 08' UTC) respect to C_{lag} whereas it came 07' earlier (C_{lag} is 01 h 40',

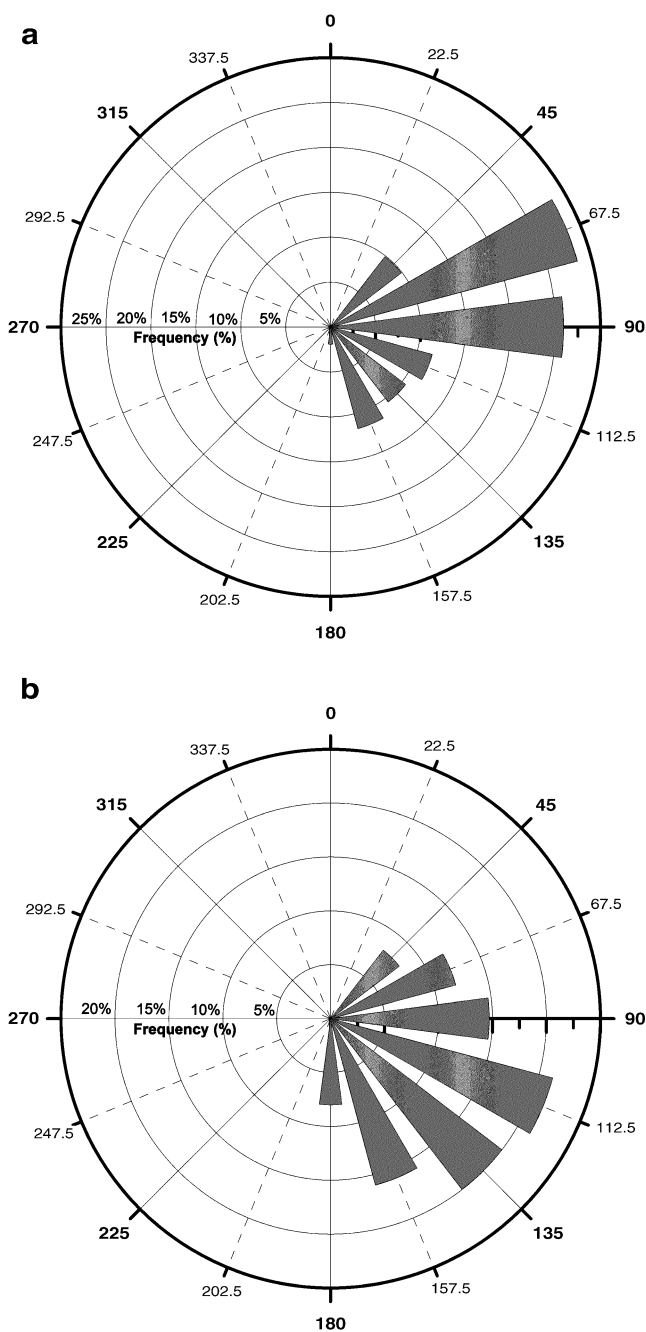


Fig. 4 Polar bar chart of the relative frequency distribution (n_i , %) of the wind direction at the time of onset for (a) onshore and (b) offshore synoptic-scale flows

i.e., until 20 h 56' UTC) for onshore geostrophic flows. Both coast-parallel flows strongly delayed the cessation of SBs: 06' for the ENE flows (C_{lag} is 1 h 53', i.e., until 21 h 10' UTC) and 15' later for the WSW winds (C_{lag} is 02 h 02', i.e., until 21 h 16' UTC) from the C_{lag} .

The detailed statistic analysis of the 8 regimes confirms these results. In Fig. 5 the four major regimes are disintegrated by means of geostrophic WS and the bar graph shows the desviations of the C_{lag} for each category

from the C_{lag} (in minutes). The light to moderate onshore winds clearly shows an earliest SB cessation of 12' (C_{lag} is 01 h 35', i.e., until 20 h 51' UTC) in relation to the average, whereas the strong supporting flows display 03' of delay (C_{lag} is 01 h 50', i.e., until 21 h 06' UTC) from the mean C_{lag} . Alternatively the light to moderate offshore components delayed the mean cessation of the SB with 09' (C_{lag} is 01 h 56', i.e., until 21 h 09' UTC), whereas strong background flows produced an early SB cessation by 03' (C_{lag} is 01 h 44', i.e., until 21 h 00' UTC) in accordance with the hypothesis put forward. For the coast-parallel large-scale winds, WS played an important role, further delaying the SB cessation 30' for the strong ENE flows (C_{lag} is 02 h 17', i.e., until 21 h 45' UTC) and 03' for the light to moderate ENE winds (C_{lag} is 01 h 50', i.e., until 21 h 04' UTC) with respect to the mean C_{lag} . In contrast, for the WSW flows the delay occurred under light to moderate flows by 27' (C_{lag} is 02 h 14', i.e., until 21 h 24' UTC), whereas the strong WSW winds scarcely displayed delay (C_{lag} is 01 h 46', i.e., until 21 h 05' UTC).

3.3 Mean duration of the SB flow (D_t)

The mean D_t is 12 h 09' and is comparable to other SB studies focused on the Western Mediterranean basin (Redaño et al. 1991; Furberg et al. 2002). With respect to the mean, the D_t for offshore synoptic-scale flows is 05' longer (12 h 14') and it shorter for onshore large-scale winds by 03' (12 h 06'). The coast-parallel flows from the WSW displayed the longest D_t (12 h 16', i.e., 07' above the mean) whereas the antiperpendicular winds from the ENE were associated with the shortest D_t (12 h 04', i.e., 05' below the mean).

Figure 6 displays the deviations of the temporal dimensions for the 8 regimes from their average. The D_t was 12' shorter under strong offshore winds (11 h 57') and 08' longer (12 h 17') for light to moderate offshore flows aloft. On the other hand, strong onshore flows tended to increase the D_t to 12 h 23' (i.e., 24' above the mean), whereas light to moderate supporting winds decreased the D_t to 11 h 57' (i.e., 12' below the mean). These results can be explained by mechanism described in sections 3.1 and 3.2. The maximum D_t occurred under strong coast-parallel geostrophic flows from the ENE (12 h 30', i.e., 21' above mean), whereas light to moderate winds from the ENE shortened the D_t with 09' below the mean (12 h 00'). Both light to moderate and strong coast-parallel flows from the WSW tended to slightly extend the D_t by 09' (12 h 18') and 05' (12 h 14') above the mean, respectively.

3.4 Mean maximum velocity of the SB (WS_{max})

The velocity of SBs near the surface is strongly influenced by the large-scale wind aloft. The average of the daily

Table 2 Distribution of the relative frequencies (n_i , %) for the eight major regimes by means of O_{wd} at the time of SB passage. The maximum relative frequencies are shown in bold type

Flow regime	45.0°	67.5°	90.0°	112.5°	135.0°	157.5°	180.0°
Offshore - Lm	8.2	13.1	14.8	21.3	14.8	18.0	9.8
Offshore - Str	7.1	7.1	14.3	21.4	42.9	7.1	0.0
Onshore - Lm	8.3	30.3	22.9	14.7	8.3	13.8	1.8
Onshore - Str	13.2	24.5	32.1	5.7	15.1	7.5	1.9
Parallel ENE - Lm	0.0	23.1	7.7	38.5	15.4	15.4	0.0
Parallel ENE - Str	0.0	0.0	50.0	0.0	0.0	0.0	50.0
Parallel WSW - Lm	8.7	13.0	21.7	21.7	21.7	8.7	4.3
Parallel WSW - Str	5.9	29.4	11.8	23.5	11.8	5.9	11.8

WS_{max} for all SB episodes is 7.11 m s^{-1} , and the absolute maximum and minimum SB gust speed are 11.61 m s^{-1} and 4.92 m s^{-1} , respectively. These figures tally well with other SB studies (Prtenjak and Grisogono 2007). The WS_{max} of the SB is 0.21 m s^{-1} stronger for offshore synoptic-scale winds (7.31 m s^{-1} , i.e., 0.20 m s^{-1} above the mean) than onshore large-scale flows (7.10 m s^{-1} , i.e., 0.01 m s^{-1} below the mean) in accordance with the hypothesis formulated. The lowest WS_{max} occurred under coast-parallel flows from the WSW (6.78 m s^{-1} , i.e., 0.33 m s^{-1} below the mean), whereas the antiperpendicular ENE flows were associated with a mean WS_{max} of 7.12 m s^{-1} (i.e., 0.01 m s^{-1} above the mean).

Figure 7 shows the deviations between the WS_{max} for the 8 regimes and their average. WS_{max} was much higher under light to moderate offshore flows (7.35 m s^{-1} , i.e., 0.24 m s^{-1} above the mean) than strong offshore winds (7.12 m s^{-1} , i.e., 0.01 m s^{-1} above the mean). In contrast, WS_{max} was much higher under strong onshore flows (7.35 m s^{-1} , i.e., 0.24 m s^{-1} above the mean) than under light to moderate onshore ones (6.98 m s^{-1} , i.e., 0.13 m s^{-1}

below the mean), which shows that strong onshore flows strengthened local wind circulation. The most intense SBs occurred under strong coast-parallel flows from the ENE (7.60 m s^{-1} , i.e., 0.49 m s^{-1} above the mean), whereas light to moderate synoptic-scale flows coming from the same compass point weakened the WS_{max} (7.04 m s^{-1} , i.e., 0.07 m s^{-1} below the mean). The weakest mean SB gust speed happened under both light to moderate (6.74 m s^{-1} , i.e., 0.37 m s^{-1} above the mean) and strong (6.83 m s^{-1} , i.e., 0.28 m s^{-1} above the mean) coast-parallel winds from the WSW. The summer vertical stability and the upper stable layers act as a strong damping mechanism (Atkinson 1981). The low level thermal inversions associated with WSW flows and the continental tropical air masses (cT) from Africa disable SB development in the Western Mediterranean area (Ramis et al. 1990).

3.5 Mean inland propagation of the SB (SB_{ext})

The intensity and rate of inland penetration of SBs are strongly modulated by large-scale flows (Tijm 1999;

Fig. 5 Deviation of the mean lags of SB cessation for the eight synoptic-scale flows from the mean C_{lag} . The wind regimes shown along the X axis are the same as in Fig. 2

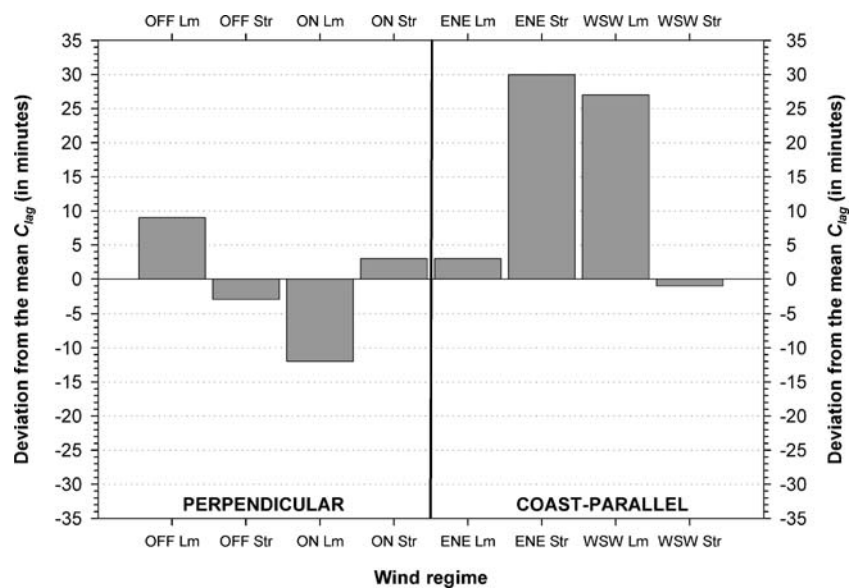
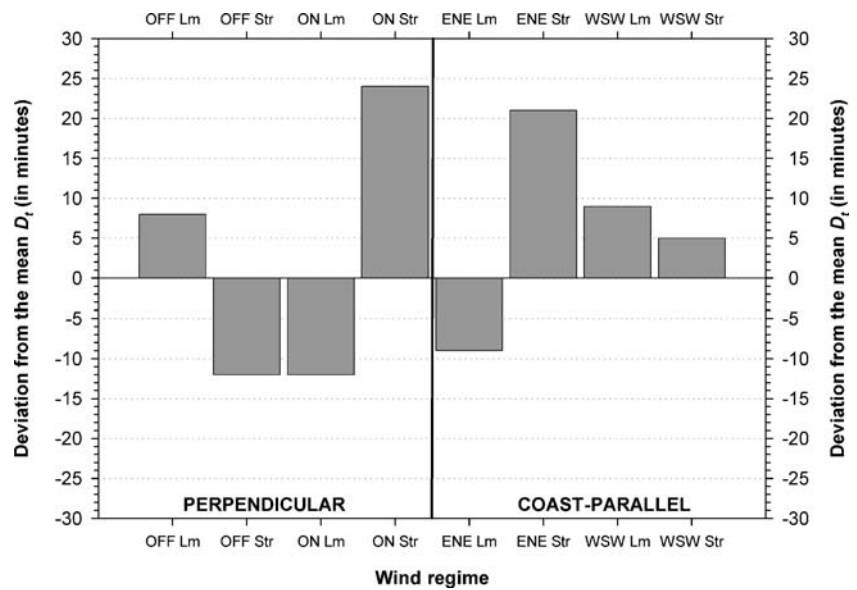


Fig. 6 Deviation of the mean duration of SBs for the eight synoptic-scale flows from the mean D_i . The wind regimes shown along the X axis are the same as in Fig. 2



Weaver 2006). The mean SB_{ext} is 114.1 km for all the selected SB days. The SB_{ext} was slightly greater for onshore wind cases (116.3 km, i.e., 2.2 km above the mean) than offshore background flows (115.5 km, i.e., 1.4 km above the mean). For instance, the maximum SB propagation (224.7 km, July 12th 2003) corresponded to a light to moderate onshore flow aloft (4.1 m s^{-1}), i.e., perpendicular onshore winds blowing in the main SB direction at the RS. The minimum SB penetration (68.2 km, June 23rd 2001) also occurred under an onshore light to moderate flow (3.5 m s^{-1}), but it was associated with a low level inversion of cT which disabled the SB. In contrast to perpendicular large-scale flows, coast-parallel geostrophic winds prevent the inland propagation of SBs: for the ENE flows the SB_{ext} is 111.0 km (i.e., 3.1 km below the mean)

and for the WSW winds is 103.8 km (i.e., 10.3 km below the mean).

Figure 8 shows that the inland penetration of SBs was restricted under strong offshore flows (109.0 km, i.e., 5.1 km below the mean; Bechtold et al. 1991; Arritt 1993; Tijn 1999) but it was further inland under strong onshore winds aloft (123.1 km, i.e., 9.0 km above the mean). However, it is found that the light to moderate offshore winds also enhanced the inland propagation of this local wind (117.0 km, i.e., 2.9 km above the mean) through compressing the horizontal land-sea temperature gradient, whereas the inland propagation of SBs was not enhanced under light to moderate onshore winds (112.9 km, i.e., 1.2 km below the mean). The coast-parallel flows prevented the inland penetration of SBs in accordance with other

Fig. 7 Deviation of the mean maximum velocity of SBs for the eight synoptic-scale flows from the mean WS_{max} . The wind regimes shown along the X axis are the same as in Fig. 2

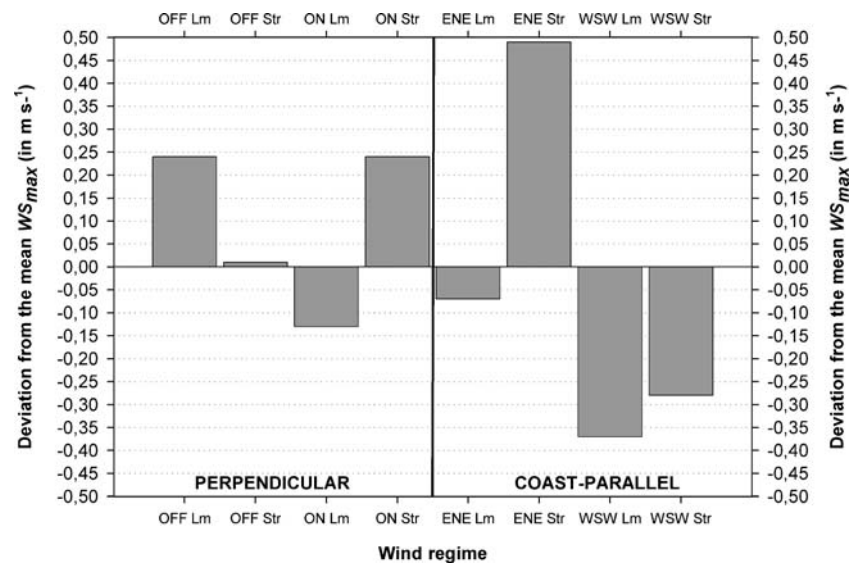
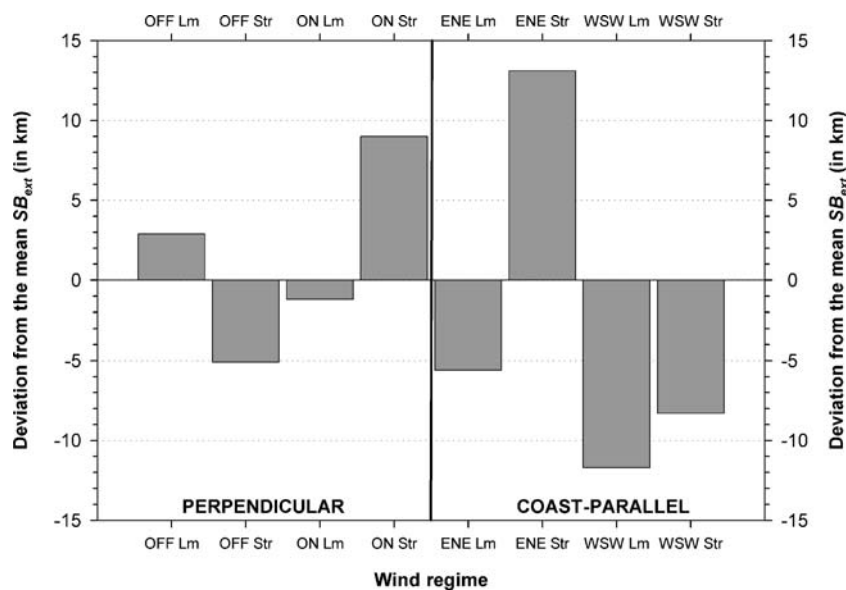


Fig. 8 Deviation of the mean inland penetration of SBs for the eight synoptic-scale flows from the mean SB_{ext} . The wind regimes shown along the X axis are the same as in Fig. 2



modelling results: the SB_{ext} is 108.5 km (i.e., 5.6 km below the mean) for the light to moderate ENE flows, 102.4 km (i.e., 11.7 km below the mean) for the light to moderate WSW winds and 105.8 km (i.e., 8.3 km below the mean) for the strong WSW flows aloft. A different behaviour is found for the strong coast-parallel flows from the ENE, which represents the most important component enhancing the horizontal extension of the SB (127.2 km, i.e., 13.1 km above the mean).

4 Summary and concluding remarks

This climatological study focused on the effect of prevailing synoptic-scale flows on the evolution of SBs. A large dataset including 292 SB days was constructed for a 6-year period (2000–2005) in the Bay of Alicante. We focused on the episodes in which the SBs reached the reference station in the May–August period. The large-scale wind was obtained from daily reanalysis data (NCEP/NCAR) at 850 hPa. The wind regimes were classified into four groups. These regimes were also sub-classified into light to moderate ($\leq 5.14 \text{ m s}^{-1}$) and strong flows ($> 5.14 \text{ m s}^{-1}$). From the selected SB dataset, the following major findings were provided:

- The arrival of SBs is delayed under strong offshore and synoptic-scale flows from the ENE. In contrast, an early SB onset is developed during strong onshore and WSW flows.
- The most intense SB passages occur under offshore large-scale flows. The opposing flows tend to strengthen mean wind speed at the time of onset, whereas onshore ambient winds, coast-parallel flows from the

ENE and the WSW appear to weaken wind speed at the time of onset, although the difference is small.

- The onshore synoptic-scale flows produce an SB onset from the 1st quadrant (from 45° to 90°) and the offshore winds from the 2nd one (from 112.5° to 157.5°). The direction of the SB start is from the ESE (112.5°) for both coast-parallel flows.
- Termination of the SB tends to be delayed under light to moderate offshore winds, strong coast-parallel wind from the ENE and light to moderate WSW synoptic flows, whereas it often comes earlier under light to moderate onshore geostrophic flows.
- The mean duration of the SB is longer for offshore than for onshore synoptic-scale winds, and the WSW and the ENE flows display the longest and shortest duration time, respectively. Strong large-scale flows extend the mean daily duration of this local wind, except for the offshore conditions.
- The mean maximum velocity of the SB is stronger under offshore than onshore large-scale flows. The most intense SBs occur under strong flows from the ENE, whereas the light to moderate winds from the WSW produce the lowest mean maximum velocities.
- The mean inland penetration of the SB is greater under strong onshore winds than strong offshore flows. The coast-parallel flows from the WSW prevent the inland propagation of this local wind, whereas the strong ENE winds represent the most important regime enhancing the horizontal extension of SBs.

Although the results are site-specific, these major findings may not be very different for other sites, as has been shown by some existing numerical studies. However, the dramatic impact of coastline curvature and coastal hills

on the characteristics of the SB (McPherson 1970; Pielke 1974; Neumann and Mahrer 1974; Mahrer and Pielke 1976), require further study using more SB episodes and numerical simulations.

Acknowledgements The Fundacion CEAM is financed by the Generalitat Valenciana and BANCAIXA. This research has been undertaken in the frame of the CONSOLIDER-INGENIO 2010 Programme (GRACCIE project). The study was supported by Spain's Education and Science Ministry (MEC) project IPIBEX (CGL2005-07664-C02-01). The authors would like to thank the NCEP/NCAR Reanalysis project for providing the upper air observations. Comments on an earlier version of this paper from anonymous reviewers are greatly appreciated.

References

- Abbs DJ (1986) Sea breeze interactions along a concave coastline in southern Australia: observations and numerical modelling study. *Mon Wea Rev* 114:831–848, (DOI 10.1007/s10546-007-9185-6)
- Arriitt RW (1993) Effects of the large-scale flow on characteristics features of the sea breeze. *J Appl Meteor* 32:116–125, (DOI 10.1007/s10546-007-9185-6)
- Asimakopoulos DN, Helmis CG, Papadopoulos KH, Kalogiros JA, Kassomenos P, Petrakis M (1999) Inland propagation of sea breeze under opposing offshore wind. *Meteorol Atmos Phys* 70:97–110, (DOI 10.1007/s007030050027)
- Atkins NT, Wakimoto RM (1997) Influences of the synoptic-scale flow on sea breezes observed during CAPE. *Mon Wea Rev* 125:2112–2130, (DOI 10.1007/s10546-007-9185-6)
- Atkinson BW (1981) Meso-scale atmospheric circulations. Academic Press, London, p 495
- Azorin-Molina C (2007) A climatological study of sea breezes in Alicante. Sea breeze fronts over the Iberian Mediterranean area and the isle of Mallorca. University Institute of Geography, University of Alicante, Alicante, Spain, p 288
- Azorin-Molina C, Martin-Vide J (2007) Methodological approach to the study of the daily persistence of the sea breeze in Alicante (Spain). *Atmosfera* 20:57–80
- Baker RD, Lynn BH, Boone A, Tao WK, Simpson J (2001) Influence of soil moisture, coastline curvature, and land breeze circulations on sea breeze initiated precipitation. *J Hydrometeorol* 2:193–211, (DOI 10.1007/s10546-007-9185-6)
- Banta RM, Olivier LD, Levinson DH (1993) Evolution of the Monterey Bay sea-breeze layer as observed by pulsed Doppler lidar. *J Atmos Sci* 50:3959–3982, (DOI 10.1007/s10546-007-9185-6)
- Bechtold P, Pinty JP, Mascart P (1991) A numerical investigation of the influence of large-scale winds on sea breeze and inland breeze type circulations. *J Appl Meteor* 30:1268–1279, (DOI 10.1007/s10546-007-9185-6)
- Bonnardot V, Planchon O, Cautenet S (2005) Sea breeze development under an offshore synoptic wind in the South-Western Cape and implications for the Stellenbosch wine-producing area. *Theor Appl Climatol* 81:203–218, (DOI 10.1007/s00704-004-0087-y)
- Borne K (1998) Observational study of sea and land breeze on the Swedish west coast with focus on an archipelago. A34, Department of Earth Sciences, Gothenburg University, Sweden: Gothenburg
- Borne K, Chen D, Nunez M (1998) A method for finding sea breeze days under stable synoptic conditions and its application to the Swedish west coast. *Int J Climatol* 18:901–914, (DOI 10.1007/s10546-007-9185-6)
- Bowers LA (2004) The effect of sea surface temperature on sea breeze dynamics along the coast of New Jersey. Graduate School-New Brunswick Rutgers, The State University of New Jersey, USA: New Brunswick
- Carnesoltas M (2002) La circulación local de brisa de mar y tierra. *Conceptos fundamentales. Rev Cub Meteor* 9:39–60
- Connell BH, Gould KJ, Purdom JFW (2001) High-resolution GOES-8 visible and infrared cloud frequency composites over northern Florida during the summers 1996–1999. *Wea Forecast* 16:713–724, (DOI 10.1007/s10546-007-9185-6)
- Darby LS, Banta RM, Pielke RA (2002) Comparisons between mesoscale model terrain sensitivity studies and Doppler lidar measurements of the sea breeze at Monterey Bay. *Mon Wea Rev* 130:2813–2838, (DOI 10.1007/s10546-007-9185-6)
- Estoque MA (1962) The sea breeze as function of the prevailing synoptic situation. *J Atmos Sci* 19:244–250, (DOI 10.1007/s10546-007-9185-6)
- Frizzola JA, Fisher EL (1963) A series of sea breeze observations in the New York City area. *J Appl Meteor* 2:722–739, (DOI 10.1007/s10546-007-9185-6)
- Furberg M, Steyn DG, Baldi M (2002) The climatology of sea breezes on Sardinia. *Int J Climatol* 22:917–932, (DOI 10.1002/joc.780)
- Gilliam RC, Raman S, Niyogi DDS (2004) Observational and numerical study on the influence of large-scale flow direction and coastline shape on sea breeze evolution. *Bound-Layer Meteor* 111:275–300, (DOI 10.1023/B:BOUN.0000016494.99539.5a)
- Gould KJ, Fuelberg HE (1996) The use of GOES-8 imagery and RAMSDIS to develop a sea breeze climatology over the Florida panhandle. Preprint, Eighth Conference on Satellite Meteorology and Oceanography, Atlanta, GA, American Meteorological Society, pp 100–104
- Haurwitz B (1947) Comments on the sea breeze circulation. *J Atmos Sci* 4:1–8, (DOI 10.1007/s10546-007-9185-6)
- Helmis CG, Papadopoulos KH, Kalogiros JA, Soilemes AT, Asimakopoulos DN (1995) The influence of the background flow on the evolution of the Saronikos Gulf sea breeze. *Atmos Env* 29:3689–3701, (DOI 10.1016/1352 - 2310(95)00008 - M)
- Kalnay E, Coauthors (1996) The NCEP/NCAR 40-year reanalysis project. *Bull Am Meteorol Soc* 77:437–471, (DOI 10.1007/s10546-007-9185-6)
- Kusuda M, Alpert P (1983) Anti-clockwise rotation of the wind hodograph. Part 1. Theoretical study. *J Atmos Sci* 40:487–499, (DOI 10.1007/s10546-007-9185-6)
- Kwiatkowski JJ (1999) Observations and analysis of the New Jersey sea breeze. Ms. Thesis, The Graduate School, Rutgers University, 79 pp
- Laird NF, Kristovich DAR, Liang X-Z, Arriitt RW, Labas K (2001) Lake Michigan lake breezes: climatology, local forcing, and synoptic environment. *J Appl Meteor* 40:409–424, (DOI 10.1007/s10546-007-9185-6)
- Mahrer Y, Pielke RA (1976) Numerical simulation of air flow over Barbados. *Mon Wea Rev* 104:1392–1402, (DOI 10.1007/s10546-007-9185-6)
- McPherson RB (1970) A numerical study of the effect of a coastal irregularity on the sea breeze. *J Appl Meteor* 9:767–777, (DOI 10.1007/s10546-007-9185-6)
- Miao J-F, Kroon LJM, Vilà-Guerau de Arellano J, Holtslag AAM (2003) Impacts of topography and land degradation on the sea breeze over eastern Spain. *Meteorol Atmos Phys* 84:157–170, (DOI 10.1007/s00703 - 002 - 0579 - 1)
- Neumann J, Mahrer Y (1974) A theoretical study of the sea and land breezes of circular islands. *J Atmos Sci* 31:2027–2039, (DOI 10.1007/s10546-007-9185-6)
- Nuss WA (2005) Coastal meteorology. Course notes for MR4240, Naval Postgraduate School, California, USA: Monterey, 68 pp
- Pielke RA (1974) A three-dimensional numerical model of the sea breezes over south Florida. *Mon Wea Rev* 102:115–139, (DOI 10.1007/s10546-007-9185-6)

- Prtenjak MT, Grisogono B (2007) Sea/land breeze climatological characteristics along the northern Croatian Adriatic coast. *Theor Appl Climatol* 91:1–15, (DOI [10.1007/s00704-006-0286-9](https://doi.org/10.1007/s00704-006-0286-9))
- Ramis C, Alonso S (1988) Sea breeze convergence line in Mallorca. A satellite observation. *Weather* 43:288–293
- Ramis C, Romero C (1995) A first numerical simulation of the development and structure of the sea breeze on the island of Mallorca. *Ann Geophysicae* 13:981–994
- Ramis C, Jansà A, Alonso S (1990) Sea breeze in Mallorca. A numerical study. *Meteorol Atmos Phys* 42:249–258, (DOI [10.1007/BF01314828](https://doi.org/10.1007/BF01314828))
- Redaño A, Cruz J, Lorente J (1991) Main features of the sea breeze in Barcelona. *Meteorol Atmos Phys* 46:175–179, (DOI [10.1007/BF01027342](https://doi.org/10.1007/BF01027342))
- Salvador R (1999) Análisis y modelización de los procesos atmosféricos durante condiciones de brisa en la costa mediterránea occidental: Zona de Castellón. Ph.D. Thesis, Technical University of Catalonia, Spain: Barcelona
- Salvador R, Millan M (2003) Análisis histórico de las brisas en Castellón. *Tethys* 2:37–51
- Savijärvi H, Alestalo M (1988) The sea breeze over a lake or gulf as the function of the prevailing flow. *Beitr Phys Atmos* 61:98–104
- Simpson JE (1994) Sea breeze and local wind. Cambridge University Press, Cambridge, p 234, (DOI [10.2277/0521452112](https://doi.org/10.2277/0521452112))
- Simpson JE, Mansfield DA, Milford JR (1977) Inland penetration of sea breeze fronts. *Quart J Roy Meteor Soc* 103:47–76, (DOI [10.1256/smsqj.43503](https://doi.org/10.1256/smsqj.43503))
- Stull RB (1995) *Meteorology today for scientists and engineers*. West Publishing Company, St. Paul, p 385
- Tijm ABC (1999) *Sea-breeze studies*. Faculteit der Natuur, University of Utrecht, Universal Press, Utrecht, p 154
- Walsh JE (1974) Sea-breeze theory and applications. *J Atmos Sci* 31:2012–2026, (DOI [10.1007/s10546-007-9185-6](https://doi.org/10.1007/s10546-007-9185-6))
- Weaver JC (2006) The impact of synoptic-scale flow on sea breeze front propagation and intensity at Eglin air force base. Masters Thesis, Naval Postgraduate School, California, USA: Monterey, 92 pp
- Wexler R (1946) Theory and observations of land and sea breezes. *Bull Am Meteorol Soc* 27:272–287
- Yan H, Anthes RA (1986) The effect of latitude on the sea breeze. *Mon Wea Rev* 115:936–956, (DOI [10.1007/s10546-007-9185-6](https://doi.org/10.1007/s10546-007-9185-6))
- Zhong S, Takle ES (1993) The effects of large-scale winds on the sea-land-breeze circulations in an area of complex coastal heating. *J Appl Meteor* 32:1181–1195, (DOI [10.1007/s10546-007-9185-6](https://doi.org/10.1007/s10546-007-9185-6))